UNIVERSITY OF LEEDS

DOCTORAL THESIS

Simulating the thermal conductivity of lower mantle minerals

Author:
Ben TODD

Supervisor:
Dr. Stephen STACKHOUSE
Dr. Andrew M. WALKER
Dr. Jon E. MOUND

A thesis submitted in fulfillment of the requirements
for the degree of Doctor of Philosophy

in the

Institute of Geophysics and Tectonics
School of Earth and Environment

August 31, 2018

Declaration of Authorship

I, Ben TODD, declare that this thesis titled, “Simulating the thermal conductivity of lower mantle minerals” and the work presented in it are my own. I confirm that:

- This work was done wholly or mainly while in candidature for a research degree at this University.
- Where any part of this thesis has previously been submitted for a degree or any other qualification at this University or any other institution, this has been clearly stated.
- Where I have consulted the published work of others, this is always clearly attributed.
- Where I have quoted from the work of others, the source is always given. With the exception of such quotations, this thesis is entirely my own work.
- I have acknowledged all main sources of help.
- Where the thesis is based on work done by myself jointly with others, I have made clear exactly what was done by others and what I have contributed myself.

Signed:

Date:

Do it!
Just do it!

Don't let your dreams be dreams.
Yesterday you said tomorrow, so just do it!
Make your dreams come true!
Just do it!

Some people dream of success,
while you're gonna wake up,
and work hard at it!
Nothing is impossible!

You should get to the point,
where anyone else would quit,
and you're not going to stop there.
No, what are you waiting for?

Do it!
Just do it!
Yes you can!
Just do it!

If you're tired of starting over,
stop giving up.

Shia LeBeouf

UNIVERSITY OF LEEDS

Abstract

Faculty of Environment
School of Earth and Environment

Doctor of Philosophy

Simulating the thermal conductivity of lower mantle minerals

by Ben TODD

The Thesis Abstract is written here (and usually kept to just this page). The page is kept centered vertically so can expand into the blank space above the title too…

Acknowledgements

The acknowledgments and the people to thank go here, don’t forget to include your project advisor…
Everyone is smart, set yourself apart by being kind.

Contents

Declaration of Authorship iii

Abstract vii

Acknowledgements ix

1 Introduction 1
- 1.1 Why is thermal conductivity important? 1
  - 1.1.1 Man-made applications 1
  - 1.1.2 In the context of the Earth 1
- 1.2 What is thermal conductivity? 1
  - 1.2.1 What affects it? 1
  - 1.2.2 Mechanisms of heat transport 1
- 1.3 Previous work - geophysics 2
  - 1.3.1 Mantle/core dynamics 2
  - 1.3.2 Thermal conductivity of the lower mantle 2
- 1.4 Thesis outline 3
  - 1.4.1 Aims 3
  - 1.4.2 Objectives 3

2 Intro/Background/Theory 2 5
- 2.1 Atomic-scale modelling 5
  - 2.1.1 Molecular dynamics 5
    - Parameter drift/convergence 5
  - 2.1.2 Interatomic potentials / Atomic interactions? 5
  - 2.1.3 LAMMPS 6
  - 2.1.4 DFT/other 6
- 2.2 Computing thermal conductivity 6
  - 2.2.1 Finite-size effects 6
  - 2.2.2 Direct method 7
    - System setup 7
    - Data processing 8
    - Finite-size effects 8
    - Other NEMD 9
  - 2.2.3 Green-Kubo 10
  - 2.2.4 Other 11
- 2.3 Previous work 11
  - 2.3.1 Method comparison 11
  - 2.3.2 Finite-size effects 11
    - STUFF THAT MIGHT BE WRONG BECAUSE FSE? 11

3 Constraining the finite-size effects of molecular dynamics methods to compute thermal coductivity 13
  3.1 Introduction . . . 13
    3.1.1 Finite-size effects . . . 13
  3.2 Computational approaches . . . 14
    3.2.1 Direct method . . . 14
    3.2.2 Green-Kubo . . . 14
  3.3 Results . . . 15
    3.3.1 Green-Kubo . . . 15
    3.3.2 Direct method . . . 16
  3.4 Summary . . . 16

4 Modelling the thermal conductivity of (Mg,Fe)SiO$_3$ at the CMB 19
  4.1 Simulating the effect of atomic impurities . . . 19
    4.1.1 How does iron behave? . . . 19
    4.1.2 Where do the impurities go? . . . 20
  4.2 Making the mantle model . . . 20
    4.2.1 Fitting the data . . . 21
      Compositional dependence . . . 21
      Temperature dependence . . . 25
  4.3 Results . . . 27

5 Modelling the lower mantle with variable thermal conductivity 29
  5.1 Main Section 1 . . . 29
    5.1.1 Subsection 1 . . . 29

6 Summary/Discussion/Conclusion 31
  6.1 Main Section 1 . . . 31
    6.1.1 Subsection 1 . . . 31

A Frequently Asked Questions 33
  A.1 How do I change the colors of links? . . . 33

Bibliography 35

List of Figures

2.1 The unit cell represents the smallest box of atoms that can be replicated to produce a crystal structure. A supercell is an arrangement of unit cells. 7
2.2 Movement and distribution of heat in the direct method. Orange to white scale represents temperature (modified from Stackhouse et al., 2015). 8
2.3 Idealised example of linear extrapolation procedure. Inverse computed conductivities are plotted against inverse simulation lengths. Extrapolation to y-axis gives conductivity of an infinite system length, i.e. the bulk material. 9
2.4 Normalised ACF. Correlation is taken over a longer length than shown on this plot (100 ps), however the function decays to less than 1% of its initial value at 2 ps. It continues to oscillate about zero, with a positive average value. 10
2.5 Integrated ACF, multiplied by constants to get thermal conductivity. Large variation in the first 1 ps corresponds to the correlation time where the ACF is unconverged (still decaying / large oscillations). Thermal conductivity is averaged from correlation time of 5 ps - 10 ps (region in red box). 11

4.1 Each coloured dot series relates to a given temperature, the dotted fit lines are the model output. 22
4.2 Modelled conductivity, shown plotted against temperature and composition. Note the sensitivity of the colour scale, showing low conductivities as dominant at high temperatures and intermediate compositions. High values are found only at low temperatures, and even then they rapidly decay and saturate to <8Wm^{-1}K^{-1}. Such conditions are unphysical at 136 GPa within the lower mantle. 23
4.3 The fit χ values plotted against T, with power law (left) and 4th order polynomial (right) trendlines. Blue and orange series are the exponential and power law fits obtained from plotting χ^T/T (see Figure 4.4). 24
4.4 Exponential fit in blue (more curved), power law in orange (flatter) . . 24
4.5 26
4.6 Number of atoms is kept constant for all volumes, data is obtained from GK calculations of a 4x4x3 simulation cell. Magnitude of volume isn't of interest, just the relative difference to the reference volume. . . 26
4.7 Data points are GK conductivity results, dotted line is the fit from Equation 4.8. 27
4.8 CAPTION 28
4.9 CAPTION 28

List of Tables

List of Abbreviations

CMB	**C**ore-**m**antle **b**oundary
LLSVP	**L**arge, **l**ow-**s**hear-**v**elocity **p**rovince
ULVZ	**U**ltra **l**ow **v**elocity **z**one
DAC	**D**iamond **a**nvil **c**ell
$\mathbf{MgSiO_3}$	Magnesium Silicate
$\mathbf{FeSiO_3}$	Iron Silicate
bdg	**b**ri**dg**manite
pv	**p**ero**v**skite
ppv	**p**ost-**p**ero**v**skite
LAMMPS	**L**arge-scale **A**tomic/**M**olecular **M**assively **P**arallel **S**imulator
DFT	**D**ensity **F**unctional **T**heory
MD	**M**olecular **D**ynamics
EMD	**E**quilibrium **M**olecular **D**ynamics
NEMD	**N**on-**e**quilibrium **M**olecular **D**ynamics
DM	**D**irect **M**ethod
GK	**G**reen-**K**ubo
ACF	**A**uto-**c**orrelation **f**unction
MFP	**M**ean **f**ree **p**ath
FSE	**F**inite-**s**ize **e**ffects
BPT	**B**allistic **p**honon **t**ransport

Physical Constants

Boltzmann constant	$k_B = 1.380\,648\,528 \times 10^{-23}\,\mathrm{J\,K^{-1}}$
Boltzmann constant	$k_B = 8.617\,330\,350 \times 10^{-5}\,\mathrm{eV/K}$

List of Symbols

a	distance	m
P	power	W (J s^{-1})
ω	angular frequency	rad

For/Dedicated to/To my…

Chapter 1

Introduction

1.1 Why is thermal conductivity important?

Knowledge of the thermal conductivity of solids is key in a wide range of technological applications and for our understanding of natural systems.

1.1.1 Man-made applications

Low thermal conductivities are required in thermoelectric materials, to maximise the efficiency of heat-electricity conversion (Snyder and Toberer, 2008).

1.1.2 In the context of the Earth

For example, in the Earth's lower mantle thermal conductivity controls the nature of planetary convection (Tosi et al., 2013), and the heat flux out of the core which powers the geotherm.

The lower mantle encompasses the region between the mantle transition zone (660 km deep, $\sim$1900 K, $\sim$25 GPa) and the CMB (2891 km deep, $\sim$4000 K, $\sim$136 GPa). The composition of this region can be approximated as 80% $MgSiO_3$/magnesium silicate perovskite (bridgmanite) and 20% MgO/magnesium oxide (periclase), both of which are insulators and past their Debye temperatures at lower mantle conditions.

1.2 What is thermal conductivity?

Thermal conductivity determines whether a material is a conductor or insulator of heat, both of which have many technological applications.

1.2.1 What affects it?

pressure, temperature, and composition

1.2.2 Mechanisms of heat transport

RADIATIVE AND ELECTRONIC TOO

Heat is transported as lattice virbrations, or phonons. The further phonons travel before scattering (mean free path, MFP) the more efficient the heat transport and thus higher the thermal condutivity. A number of effects (MENTION MATTHIESSEN'S RULE) cause phonons to scatter: (1) collisions with other phonons in the lattice, (2) boundaries or defects in the material, and (3) impurities in the atomic structure.

1.3 Previous work - geophysics

INSERT GEOPHYSICS INTRO HERE ASWELL

A range of atomic scale simulation methods are available to determine the lattice thermal conductivity of materials. These are invaluable for calculating thermal conductivity at conditions of which experiments are difficult, e.g. the extreme conditions found in the Earth's lower mantle (pressures and temperatures up to 136 GPa and 4000 K at the core-mantle boundary).

1.3.1 Mantle/core dynamics

Thermal conductivity in the deep Earth influences dynamic processes such as mantle convection and heat loss from the core (Lay et al., 2008).

1.3.2 Thermal conductivity of the lower mantle

Many studies assume lowermost mantle thermal conductivity to be 10 $Wm^{-1}K^{-1}$ (e.g. Lay et al., 2008), but uncertainty in the extrapolation of results made at low pressures and temperatures gives a range of 4 - 16 $Wm^{-1}K^{-1}$ (Brown and McQueen, 1986; Osako and Ito, 1991; Hofmeister, 1999; Goncharov et al., 2009; Manthilake et al., 2011; Ohta et al., 2012).

There have been several computational studies to calculate the lattice thermal conductivity of bridgmanite at CMB conditions. Osako and Ito (1991) measured the lattice thermal conductivity of $MgSiO_3$ perovskite, using a modified Ångstrom method. They investigated a temperature range of 160 - 340 K at ambient pressure. At 300 K, a conductivity of 5.1 $Wm^{-1}K^{-1}$was obtained. This value is similar to that reported for chemical and structural analogues, $MgSiO_3$ enstatite (5.0 $Wm^{-1}K^{-1}$REF) and $CaTiO_3$ perovskite (4 $Wm^{-1}K^{-1}$REF). The authors extrapolated the value to mantle conditions, neglecting radiative thermal conductivity. They predicted a value of 3.0 $Wm^{-1}K^{-1}$just beneath the mantle transition zone at 1900 K, and 12.0 $Wm^{-1}K^{-1}$at the top of the D'' layer at 2500 K, a four-fold increase. Thermal conductivity is highlighted as an important indictor of lowermost mantle structure, whether or not the D'' layer can behave as a thermal boundary between core and mantle.

Manthilake et al. (2011) measured $MgSiO_3$ perovskite at 26 GPa and 473 - 1073 K, and periclase at 8 and 14 GPa between 373 - 1273 K. In order to estimate values of thermal conductivity at the top and bottom of D'' for a lower mantle compositional model of 4 perovskite : 1 periclase, the authors extrapolated their measurements to high temperature and pressure. For an iron-free mantle, thermal conductivities of 18.9 ± 1.6 $Wm^{-1}K^{-1}$and 15.4 ± 1.4 $Wm^{-1}K^{-1}$are estimated for the top of D'' and CMB respectively. Similarly, for a mantle composition with Fe, thermal conductivities of 9.1 ± 1.2 $Wm^{-1}K^{-1}$and 8.4 ± 1.2 $Wm^{-1}K^{-1}$are calculated. This highlights the importance of impurities in controlling thermal conductivity in the lower mantle.

Ohta et al. (2012) measured the lattice thermal diffusivity of $MgSiO_3$ perovskite and post-perovskite at room temperature and pressures up to 144 GPa (using a diamond-anvil cell (DAC) and light heating thermoreflectance). These results suggest a perovskite-dominant lowermost mantle would have conducitivity of around 11 $Wm^{-1}K^{-1}$, and that parts of the lowermost mantle where post-perovskite is stable will have a conductivity approximately 60% higher. The authors suggest that these differences in conductivity between phases will not have a large effect on CMB heat flux, assuming the double-crossing perovskite phase model. The lattice conductivity of $MgSiO_3$ perovskite is shown to increase with pressure and decrease with temperature as expected. The inclusion of impurities is expected to decrease lattice thermal conductivity.

MANTHILAKE'S HIGH T RESULTS? CAN'T FIND REFERENCE?

My approach is similar to that of Ammann et al. (2014), who use the direct method and interatomic potentials reporting a value of $\sim$8.5 $\mathrm{Wm^{-1}K^{-1}}$. Stackhouse et al. (2015) again use the direct method but with density functional theory, yielding conductivity of 6.8 ± 0.9 $\mathrm{Wm^{-1}K^{-1}}$. Using Green-Kubo, Haigis (2013) report a value of 12.4 ± 2.0 $\mathrm{Wm^{-1}K^{-1}}$ for conditions of 3000 K, 139 GPa. Tang et al. (2014) and Dekura et al. (2013) employed first principles, anharmonic lattice dynamics techniques, obtaining values of $\sim$1 $\mathrm{Wm^{-1}K^{-1}}$ (CMB conditions) and 2.3 $\mathrm{Wm^{-1}K^{-1}}$ (for 4000 K and 100 GPa) respectively. These results are much lower than other studies, and could be because of LD TRUNCATION OF CONDUCTIVITY [CRITICAL ANALYSIS].

1.4 Thesis outline

In Chapter 2 we provide an overview of the methods and expand on issues. I outline my computational approaches, for the non-equilibrium molecular dynamics direct method and equilibrium molecular dynamics Green-Kubo method. I show convergence of computed conductivity with respect to simulation cell size and shape

In Chapter 3, PRESSURE/TEMPERATURE EFFECTS. DISCUSS [P/T] SCALING LAW / THEORETICAL MODEL

In Chapter 4, ADAPTING SYSTEM TO INCLUDE IRON, DETERMINING EFFECT OF IMPURITY CONTENT, PRODUCING A MODEL OF THE LOWER MANTLE CONDUCTIVITY WITH VARIABLE TEMPERATURE AND BRIDGMANITE COMPOSITION

1.4.1 Aims

1.4.2 Objectives

Chapter 2

Intro/Background/Theory 2

2.1 Atomic-scale modelling

Knowledge of thermal conductivity is important for modelling the deep earth, but can not be measured experimentally at core mantle boundary conditions. Atomic scale simulations sidestep experimental limitations, but system size must be chosen carefully in order to determine accurate conductivity values. Classical molecular dynamics approaches are utilised, with the intention of constraining appropriate system parameters.

A range of atomic scale simulation methods are available to determine the lattice thermal conductivity of materials. These are invaluable for calculating thermal conductivity at conditions of which experiments are difficult, e.g. the extreme conditions found in the Earth's lower mantle (pressures and temperatures up to 136 GPa and 4000 K at the core-mantle boundary).

2.1.1 Molecular dynamics

Parameter drift/convergence

We ensure all calculations are run for a sufficient length of time for the conductivity value to converge. When conductivity fails to converge it means either the simulations needs to be run for longer (unlikely with our nanosecond-scale classical calculations), or the system temperature has drifted. When NVE simulations are run for a long time there is noticable drift in the average system temperature (due to numerical approximations in the equation of motion), which in turn causes drift in the computed conductivity.

NPT-NVT-NVE PROCESS

2.1.2 Interatomic potentials / Atomic interactions?

With the interatomic potential of Oganov et al. (2000) we simulate bridgmanite ($MgSiO_3$ perovskite). To assess finite-size effects we use larger simulation cells than those employed in previous studies. The atom counts associated with these cells (the largest cell considered having over 100,000 atoms) means an ab initio study would be impractical, necessitating the use of interatomic potentials. We expect the potentials to represent the finite size effects well, even if computed conductivities may inaccurate compared to first-principles calculations.

WHY OGANOV?

WHAT CUTOFFS?

2.1.3 LAMMPS

LAMMPS (Large-scale Atomic/Molecular Massively Parallel Simulator) is a classical molecular dynamics code (Plimpton, 1995).

2.1.4 DFT/other

Required? Subsubsection somewhere?

2.2 Computing thermal conductivity

Stackhouse and Stixrude (2010) review different methods to compute thermal conductivity, in the present work we focus on two of these: (1) Equilibrium molecular dynamics based on the Green-Kubo relations to determine the thermal conductivity from heat flux fluctuations and their time-dependence (Green, 1954; Kubo, 1957; Kubo, 1966; Schelling et al., 2002). (2) The non-equilbrium molecular dynamics-based "direct method", where thermal conductivity is calculated from an imposed heat flux and corresponding temperature gradient via Fourier's Law (Müller-Plathe, 1997; Nieto-Draghi and Avalos, 2013).

2.2.1 Finite-size effects

[[[Give its own section, or as subsection in each method?]]]
Computational techniques are not limited by the reproduction of physical conditions like experiments, however they are affected by the size and shape of the simulation cell. The effects of the finite system size available for computation must be checked, as systems with too few atoms are sometimes unable to reproduce the behaviour of the bulk material. If the wavelength of a phonon is too long to fit into a cell, it is not able to transport heat like it should. In the case of the direct method, the length to cross sectional area (CSA) aspect ratio can also matter.

Considering systems of varying size, length-dependent conductivities are obtained from the direct method and extrapolated to the bulk material (Schelling et al. (2002)). The validity of this extrapolation procedure have been called into question (e.g. Sellan et al. (2010)), when a linear trend cannot be fit through the length-dependent conductivities. We describe finite-size effects (FSE) which cause the conductivity result of a simulation to diverge from the value expected by a linear trend, and offer a comparison with results obtained from the Green-Kubo method. The two methods have previously been compared (e.g. Schelling et al. (2002) [[[REFERENCED EARLIER IN THIS PARAGRAPH, THIS OKAY?]]]), and have been found to give results in good agreement.

The finite-size effects (FSE) I describe are associated with phonon-phonon scattering, or the lack thereof, and boundary-scattering or truncation of phonon mean free path due to limited system sizes. These phenomena combine to misrepresent the phonon behaviour of the bulk material.

The FSE observed for a material change with thermal conductivity/phonon MFP, and thus are pressure, temperature, and composition sensitive. Higher conductivity(or is it MFP?) materials/conditions require larger systems to eliminate FSE (and vice versa) [[[BUT IS THIS TRUE?]]].

2.2.2 Direct method

The direct method is the computational implementation of a typical experiment to measure thermal conductivity, using Fourier's law to relate heat flux (q) and temperature gradient (∇T) to thermal conductivity (k),

$$q = -k\nabla T. \tag{2.1}$$

System setup

In the direct method energy is transferred from one group of atoms to another, creating hot and cold regions between which heat flows. The resultant temperature gradient is measured by calculating the temperature of individual groups of atoms along the direction of the heat flux. Simulation cells tend to be long relative to their cross-sectional area, defined as height by width (see Figure 2.1). Cell boundaries are periodic and the hot and cold sections are half the cell length apart, meaning heat flows in both directions from hot to cold (one of which is across the length-end periodic boundary). This results in two similar temperature gradients which can be averaged.

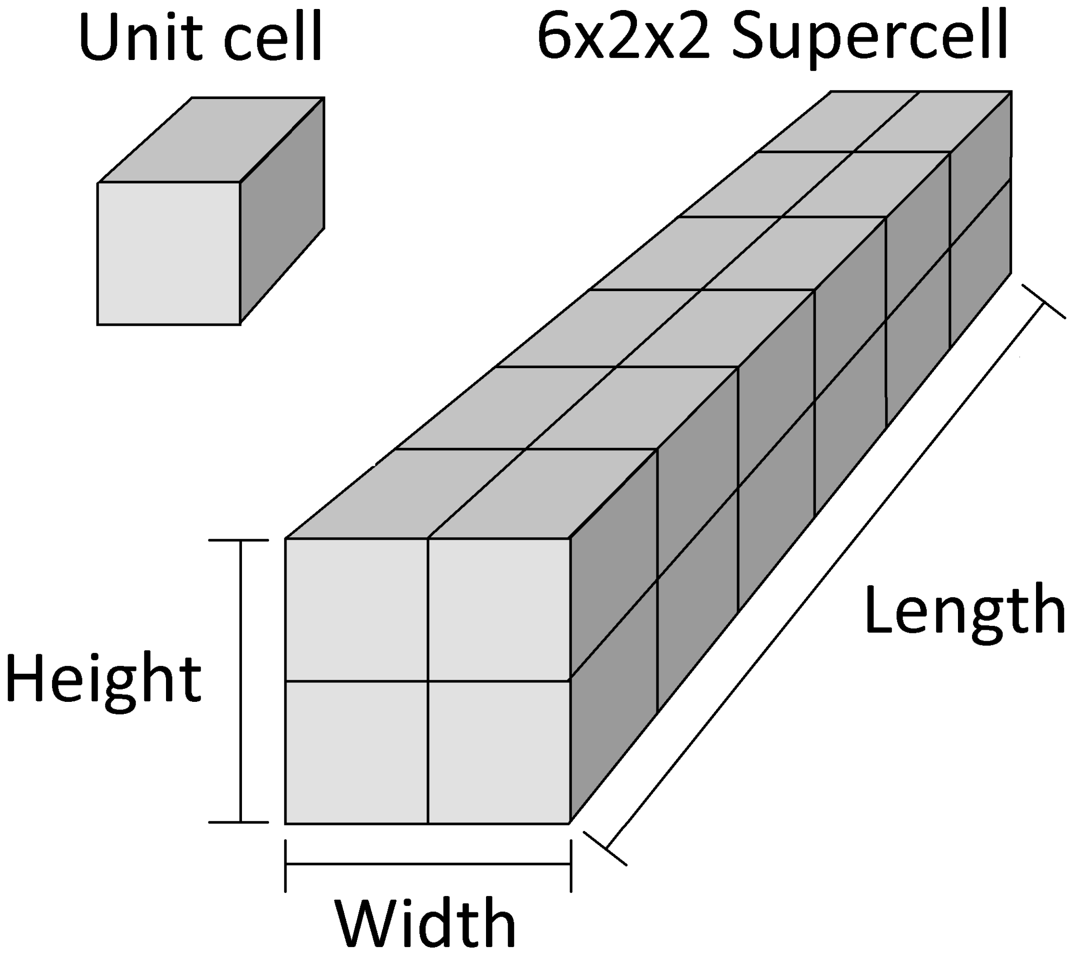

FIGURE 2.1: The unit cell represents the smallest box of atoms that can be replicated to produce a crystal structure. A supercell is an arrangement of unit cells.

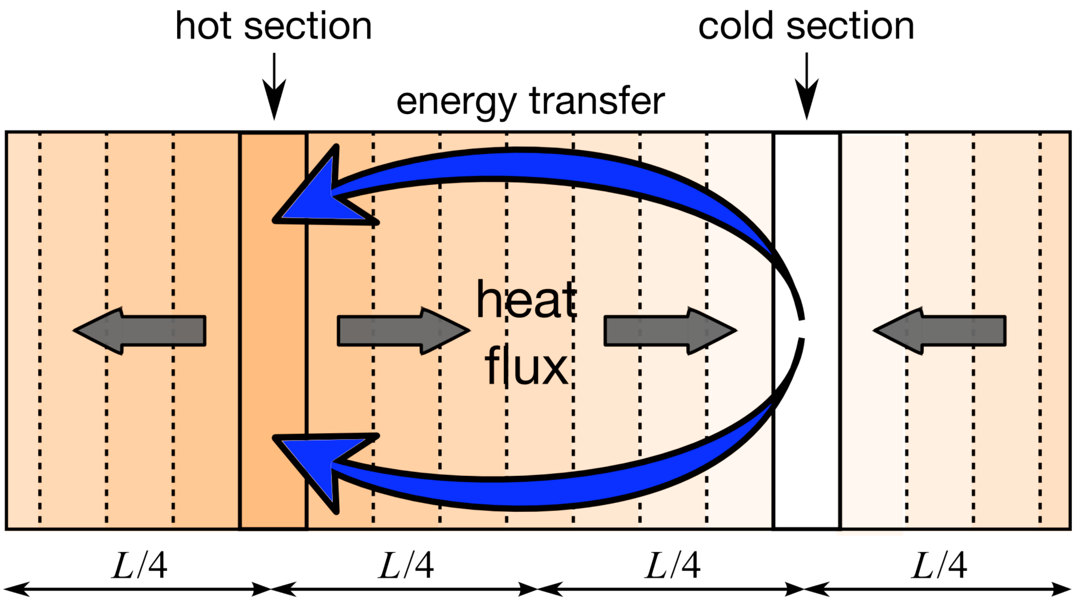

FIGURE 2.2: Movement and distribution of heat in the direct method. Orange to white scale represents temperature (modified from Stackhouse et al., 2015).

From kinetic theory [[[REF?]]], conductivities computed by the direct method (k_L) are dependent on length of simulation cell,

$$k_L = \frac{1}{3} C_V v l_L, \tag{2.2}$$

where C_v is the volumetric heat capacity, v is the average phonon drift velocity, and l_L is the phonon mean free path.

Data processing

The finite size of the simulation cell truncates the mean free path, underestimating conductivity compared to that of the bulk material (k_∞). Using results from simulations of varying cell length (L), conductivity is extrapolated to a length-independent value (where b is a material dependent parameter),

$${k_L}^{-1} = bL^{-1} + {k_\infty}^{-1}. \tag{2.3}$$

Inverse conductivities from direct method simulations are plotted against corresponding inverse cell lengths. A straight line is fit to the data and extrapolated to the y-axis (at which the inverse cell length equals zero and real length equals infinity), where the intercept gives the inverse of the bulk material conductivity (Schelling et al., 2002).

Finite-size effects

Problems arise when the data do not support a linear trend. There are two effects of finite system size that can cause an individual direct method simulation to diverge away from an inferred/expected linear trend, both of which result in overestimation of the length-dependent conductivity data point. First, when the distance between hot and cold sections (controlled by cell length) is shorter than the MFP, phonons

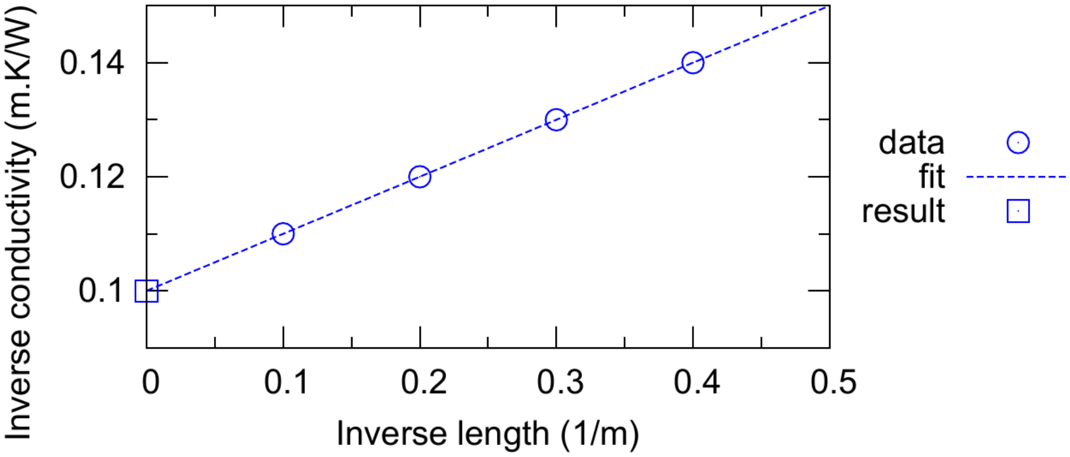

FIGURE 2.3: Idealised example of linear extrapolation procedure. Inverse computed conductivities are plotted against inverse simulation lengths. Extrapolation to y-axis gives conductivity of an infinite system length, i.e. the bulk material.

travel ballistically (i.e. without any scattering events) from heat source to sink (Sellan et al., 2010). Conductivites in shorter length cells are overestimated when this occurs, reducing the gradient of the linear fit and thus underestimating the extrapolated conductivity.

For a given length, conductivity is dependent on the CSA, or aspect ratio of the simulation cell. Conductivity is overestimated due to an underestimation of phonon-phonon scattering, from sparse phonon phase sampling in cells where cross-section is small compared to length. Phonons that aren't resolved cannot contribute to phonon-phonon scattering effects. Reduced scattering means heat transport is artificially more efficient than expected from the bulk material.

[[[SPECIFIC ALERT, REFERENCING THINGS I FOUND]]] However, the required CSA to abate this FSE is length-dependent. When the CSA is smaller than required for all cell lengths (e.g. 1x1 [FIGURE]), all conductivities are overestimated (Thomas et al., 2010, albeit for nanotube diameter?). As the CSA is increased, the data points (and thus also the extrapolated result) shift to lower conductivities (higher inverse conductivities). It is at this point that the short cells with lengths of similar order, will report conductivities converged with respect to CSA. Assuming these cells are sufficiently long to avoid the ballistic phonon transport (BPT), a linear fit can be extrapolated to obtain conductivity (for CSA around 2x2, the case at 4000 K).

The convergence is not necessarily observed concurrently for longer cells however, where they might show overestimated conductivities compared to the fit through the short cells (Hu et al., 2011). This would cause the fit to all data to be steeper than it should, increasing the extrapolated result. [[[HOPEFULLY THIS IS TRUE]]] I can show that increasing CSA does not change the computed conductivity at short lengths, but does reduce values from longer cells and bring them into alignment with the expected fit.

Other NEMD

Fixed ends?

Sinusoidal temperature perturbation.

2.2.3 Green-Kubo

The Green-Kubo method uses auto-correlation functions (ACFs) to quantify time-dependence of heat fluxes (shown in Figure 2.4, and Equation 2.4), in a simulation cell of roughly cubic dimensions (WHY??) and spatially-consistent average temperature. Instantaneous heat fluxes can be used to determine how energy is dissipated within a system, where brief flux events mean heat is transferred quickly indicating high thermal conductivity [[[and vice versa, BUT IS THIS TRUE?]]].

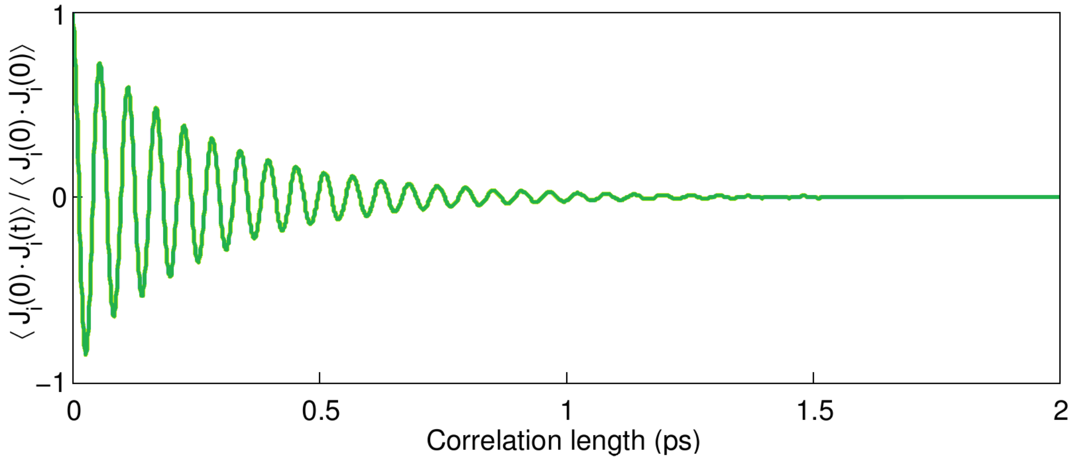

FIGURE 2.4: Normalised ACF. Correlation is taken over a longer length than shown on this plot (100 ps), however the function decays to less than 1% of its initial value at 2 ps. It continues to oscillate about zero, with a positive average value.

The auto-correlation is obtained over the net heat flux series in each crystallographic direction, for a timescale up to a chosen correlation length.

$$ACF_i = \langle J_i(0) \cdot J_i(t) \rangle \,, \tag{2.4}$$

where i specifies direction, J is heat flux, and t is the correlation length. The integral of heat flux ACF is proportional to thermal conductivity via the Green-Kubo equation (see Figure 2.5 and Equation 2.5),

$$\kappa_i = \frac{V}{k_B T^2} \int_0^\infty \langle J_i(0) \cdot J_i(t) \rangle \, dt, \tag{2.5}$$

[[[I am using "k"s and "kappa"s to represent thermal conductivity, kappa here and k earlier?]]] where V is the simulation cell volume, k_B is the Boltzmann constant, and T is the average temperature of the system. In this study we use Green-Kubo results as an independent check on the direct method, as they do not have the same finite size-effects. Obtaining a converged conductivity result simply depends on using a large enough cell volume / number of atoms.

The individual integrals obtained from the Green-Kubo show variation from the average combined integral on the order of the mean. Many simulations from different intital temperature conditions are required in order to ensure good sampling of conductivity, as well as ensuring the computation time for each is long enough for convergence. This makes Green-Kubo a computationally expensive method, especially for large systems.

The ACF should decay to zero as correlation time tends to infinity, however noise in the ACF prevents this. This will ultimately cause the integral to diverge/drift on

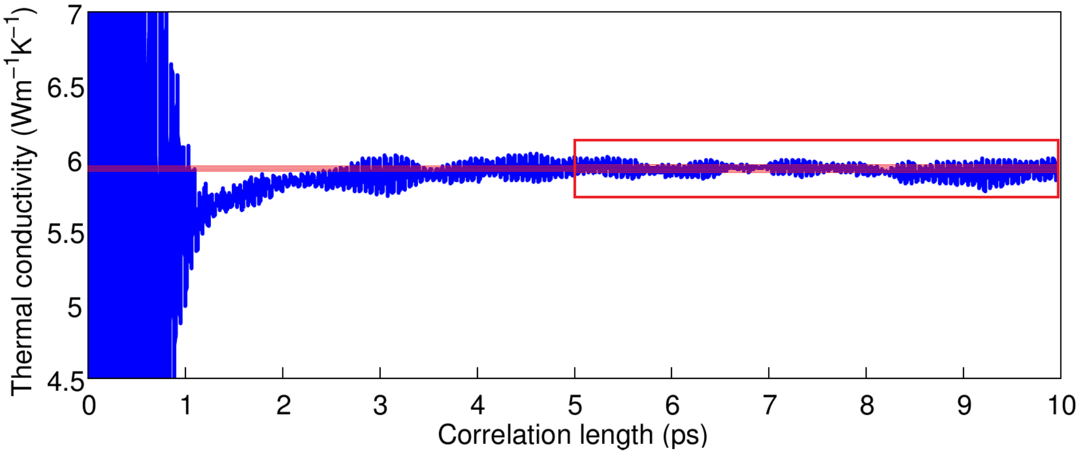

FIGURE 2.5: Integrated ACF, multiplied by constants to get thermal conductivity. Large variation in the first 1 ps corresponds to the correlation time where the ACF is unconverged (still decaying / large oscillations). Thermal conductivity is averaged from correlation time of 5 ps - 10 ps (region in red box).

long timescales. Howell (2012) fits a series of exponential decays to their ACF, forcing the expected decay to zero and subsequent (constant) integral convergence. This is represents a significant improvement on the conductivity estimate at long correlation lengths, but is mostly similar with the un-fit integrals early in the correlation. (INTEGRAL DRIFT FIGURE, JUST THE ONE INTEGRAL FOR 100PS)

(STACKHOUSE 2010 REFERENCES Volz and Chen 2000; Sun and Murthy 2006)

2.2.4 Other

(3) Anharmonic lattice dynamics (Tang and Dong, 2009).
(4) Combined quasiharmonic lattice dynamics and molecular dynamics method (Koker, 2009).

2.3 Previous work

2.3.1 Method comparison

2.3.2 Finite-size effects

Should this section be interspersed into when FSE are mentioned in methods?

STUFF THAT MIGHT BE WRONG BECAUSE FSE?

Chapter 3

Constraining the finite-size effects of molecular dynamics methods to compute thermal coductivity

3.1 Introduction

Knowledge of the thermal conductivity of solids is key in a wide range of technological applications and for our understanding of natural systems. For example, in the Earth's lower mantle thermal conductivity controls the nature of planetary convection (Tosi et al., 2013), and the heat flux out of the core which powers the geotherm. Low thermal conductivities are required in thermoelectric materials, to maximise the efficiency of heat-electricity conversion (Snyder and Toberer, 2008).

A range of atomic scale simulation methods are available to determine the lattice thermal conductivity of materials. These are invaluable for calculating thermal conductivity at conditions of which experiments are difficult, e.g. the extreme conditions found in the Earth's lower mantle (pressures and temperatures up to 136 GPa and 4000 K at the core-mantle boundary).

(MOVE - to where though?) Many studies assume lowermost mantle thermal conductivity to be 10 $\mathrm{Wm^{-1}K^{-1}}$ (e.g. Lay et al., 2008), but uncertainty in the extrapolation of results made at low pressures and temperatures gives a range of 4 - 16 $\mathrm{Wm^{-1}K^{-1}}$ (Brown and McQueen, 1986; Osako and Ito, 1991; Hofmeister, 1999; Goncharov et al., 2009; Manthilake et al., 2011; Ohta et al., 2012).

3.1.1 Finite-size effects

THE PROBLEM OF FSE IN COMPUTATIONAL TECHNIQUES

EXACERBATED BY RANGE OF LOWER MANTLE CONDITIONS

The effect of FSE on conductivity results depends on the magnitude of conductivity/phonon MFP/physical conditions. At low kappa/low MFP/high T/ (my 4000 K), no BPT is observed, and short cells (>16 unit cells) can be used for extrapolation. In fact, short cells must be used to extrapolate, unless CSA considersations are made to ensure convergence of long cell results.

At high kappa/high MFP/low T (my 1000 K), BPT must considered at the shorter cells (just 6?). Effectively there is a "sweet-spot", a window of cell lengths for a given CSA that produce consistently-converged results. Long cells outside of the window require a larger CSA, short cells outside show BPT. At 4000 K the lower limit of the window is smaller than the minimum cell length considered, and the upper limit is between 16-24 unit cells. For 1000 K the lower limit of the window moves inside the simulated cell length range around 6-8 unit cells (OR MORE?). The upper limit of the window appears to be larger than 96 unit cells, including all long cells up to this value produces an extrapolation in agreement with GK.

3.2 Computational approaches

In this section I talk about my specific approaches to applying the methods discussed in Chapter 2

3.2.1 Direct method

The simulation supercell is split into sections along its length, each half a unit cell wide. Two of these sections, half the supercell length apart, are designated as the heat source and heat sink. We measure (HOW?) the temperature in all sections to obtain the temperature gradient. Heat flows in both directions from the hot section because of cell periodicity [NEED DIRECT METHOD DIAGRAM BY THIS PARA], meaning there are two temperature gradients to average. Where L is supercell length in unit cells and S (= 2L) gives the number of sections, we obtain S/2 + 1 temperature points to fit the gradient. Because the temperature gradient is non-linear around the heat source and sink, we ignore S/12 sections (rounded to nearest integer) from both ends of the temperature gradient. For a given simulation cell we fit S/3 + 1 points to obtain the temperature gradient. We use a minimum supercell length of 6 unit cells (12 sections, 5 data points), in order for sufficient fitting of the temperature gradient. [HOW NECESSARY IS THIS PARA, VERY JARGONY]

(MOVE TO RESULTS?) Changing the width of the heated sections has no effect on the conductivity result. Furthermore, changing the width (and thus number) of temperature bins has no effect on the sampled gradient, assuming resolution is large enough to capture the non-linear region around the heat source/sink.

An important factor for utilising the direct method is maintaining a sensible temperature gradient where Fourier's law remains valid, i.e. conductivity is constant along the length of the cell. Thermal conductivity is strongly temperature-dependent at upper lower-mantle conditions (1000 K), it is therefore undesirable to have substanially different conductivities as a of function of temperature across the cell. The opposite case is also true, the difference in temperature between hot and cold sections must be larger than the uncertainty in the average system temperature.

We typically observe fluctuations in temperature of around ±50 K during temperature equilibration, and look for temperature increases/decreases on the order of 10% the mean temperature. We control the magnitude of the gradient by altering the interval at which heat is exchanged. To produce the desired gradients we find shorter intervals are required as cell length decreases, cross-sectional area increases, and system equilibrium temperature decreases.

3.2.2 Green-Kubo

The bridgmanite unit cell does not have cell dimensions resembling a cube (a:b:c = 1:1:1.4), so we use supercell structures of 3x3x2, 4x4x3, 5x5x4, 6x6x4 etc. to make an approximately cubic simulation cell. Temperature initialisation (NVT) of 1 ns is run to ensure convergence of system pressure and temperature. To obtain heat flux auto-correlation functions, a simulation for each initial temperature condition is run for X ns, with 9 successive repeats for a total of 10 jobs. This gives 10 ACFs from each initial condition. Simulation runs are split in this manner to be feasible computationally, and also to provide enough samples for ensemble averaging statistics (???).

3x3x2 - X = 10 ns, for 20 inital conditions - 2 μs total time

4x4x3 - X = 10 ns, for 30 inital conditions - 3 μs total time

5x5x4 - X = 5 ns, for 20 inital conditions - 1 μs, X = 1 ns, for 70 inital conditions - 0.7 μs, 1.7 μs total time

6x6x4 - X = 1 ns, for 80 inital conditions - 0.8 μs total time

THIS INFO IN A TABLE, OR JUST GIVE FOR THE RELEVANT VOLUME?

I DON'T LIKE THE INCLUSION OF ALL THE ABOVE INFORMATION

In this study we compute ACFs up to correlation lengths of 100 ps, with (100,000) 1 fs timesteps. This length is longer than required but selected as a proof of concept to show convergence in the conductivity result, additionally to display the extent and behaviour of drift in the integrals for long correlation times. We show in Figure **??** that the magnitude of the ACF decays to much less than 1% of its initial value around a correlation time of 1 ps, inferring the start of convergence for the integral and thus conductivity. (ACF FIGURE FOR CORREL < 10PS?, RUNNING AVERAGE SHOWS CONVERGENCE)

ACFs produced by each simulation are integrated seperately, and averaged into a single series. This process is performed for heat fluxes in each crystallographic direction, to allow analysis of anisotropy and finite system size effects. From this combined integral we pick a window of correlation lengths to capture a flat, converged region (or the section just after the 'bottleneck' if convergence is not obvious). This correlation length window is then applied to all N integrals constituent to the combined series, giving N integral averages and corresponding standard deviations. A weighted average is then taken of these data points, to give a single value with uncertainty. This value is directly proportional to thermal conductivity, as given by EQUATION XXX.

Considering bridgemanite at lower mantle conditions, we find correlation time windows in the range of 2-30 ps to be suitable. At the low-end, this allows the initial high-variability in integral value to be ignored. At the high-end, the time is long enough for good sampling of the integral, but short enough to ignore the drift-effects. The magnitude and range of the window typically increases with conductivity (or with decreasing temperature etc.), e.g. 2-10 ps at 4000 K, and 10-30 ps at 1000 K.

3.3 Results

3.3.1 Green-Kubo

A supercell volume of 3x3x2 (((REFER TO GRAPH, WILL NEED 1000K TOO))) fails to reproduce conductivities on the same order as the larger cells for all directions. We identify 4x4x3 and larger cells as being converged with respect to cell volume (((PROBLEMATIC STATEMENT, NOT CONVINCING, BY WHAT METRIC?))). This a useful result in terms of computation efficiency, as 6x6x4 supercells are 3 times as large (VOLUMOUS? REFERENCE ATOM COUNT?) as 4x4x3.

3.3.2 Direct method

When determining finite-size effects, it is important to consider the scenario with largest phonon mean-free paths. Phonon MFPs are largest at low temperatures (beyond the Debye temperature) and high pressures. In light of this we consider pressure of 136 GPa and temperatures of 1000 K and 4000 K. 136 GPa / 4000 K represents the expected conditions of the core-mantle boundary, whereas 136 GPa / 1000 K is unphysical in the context of the Earth but maximises MFP. UPDATE - GK RUINS EVERYTHING

By computing conductivities across a range of cell lengths we show that direct method simulations with small cross-sectional areas fail to produce converged results with respect to larger CSAs. Without considering any extrapolation, it is clear that small CSA cells overestimate conductivity (Figures **??** & **??**) at conditions of both 1000 K and 4000 K. On both figures the results for cells with CSA 2x2 and larger plot close to on top of each other. Producing the same results as 8x8 cells, we conclude that cells with CSA of 2x2 are suitable for direct method simulations of bridgmanite.

Now considering CSAs of 2x2, we examine the divergence of conductivity result with cell length from an expected linear trend (Figure **??**). As mentioned in Section **??**, cells that are too long or short cause a conductivity result to be overestimated. At 4000 K we find that cells up to 24 unit cells length (<0.06 in inverse length) produce a reasonably linear trend. At this condition, there is no reasonable overestimation due to short cells and ballistic phonon transport. However at 1000 K where the MFP is longer, a cell of length 6 unit cells (inverse length 0.167) produces conductivity larger than expected. The same long-cell divergence is found >24 unit cells length, the onset of insufficient phonon sampling. For all direct method simulations of bridgmanite at lower mantle conditions, we recommend employing cell lengths of 8 - <24 unit cells. Due to the increasing computational cost associated with cell length (especially for ab initio methods), we recommend the longest cells be 16 unit cells. FINITE SIZE EFFECTS INCREASE WITH MFP/KAPPA

Now we consider CSA of 2x2 and supercell lengths of 8, 10, 12, and 16 unit cells for comparison with the results from Green-Kubo. After performing a weight least squares regression (extrapolation) on the direct method results, we obtain a conductivity with uncertainty. Figure **??** shows the extrapolation and Green-Kubo result (at x = 0). They agree within error, meaning we have chosen a suitable set of criteria for working with direct method results. DO I NEED TO PROVE THAT OTHER LENGTHS/EXTRAPOLATIONS DON'T MATCH GK? FINE AT HIGH T / SHORT MFP, LOW T / HIGH MFP NEEDS LONGER CELLS TO EXTRAPOLATE, OR MORE SHORTER CELLS IGNORED.

3.4 Summary

For bridgmanite (at conditions representing the lower mantle), we show that use of the direct method for calculation of thermal conductivity will lead to an overestimate if the simulation cell is too long (>16 unit cells, 4000 ONLY!!!). Small cross-sectional areas (<2x2 unit cells) also overestimate the thermal conductivity. This informs future work using Density Functional Theory, and will allow a model of lower mantle conductivity considering composition to be established [[[OOPS]]].

(ASSUMING THE RESULTS ARE CORRECT AND AGREE WITH GK) We see the non-linear region as described by Sellan et al. (2010) for the cell length of 6 unit cells at 1000 K, which has individually higher conductivity than expected from the linear fit through data points corresponding to lengths of 8-16 unit cells. When included in the extrapolation, this reduces the gradient of the fit, raising the intercept and thus causing conductivity to be underestimated. At temperature of 4000 K, the 6 length cell is inline with the fit through other cells with length less than 16 unit cells. As the ratio of cell length to phonon MFP increases with temperature, we believe the onset of divergence as described by Sellan et al. moves to the right (??? - MENTION ACTUAL EFFECT - QUANTIFY RATHER THAN REFERENCING GRAPH). A shorter MFP needs shorter cell lengths to display divergent conductivity, of which we have not sampled (at high temperature). DOING THE DIRECT METHOD WITH CELLS OF LENGTH LESS THAN 6 UNIT CELLS AT ANY TEMPERATURE IS A BAD IDEA BECAUSE ...

We find conductivity is definitely dependent on CSA, but we were not able to increase CSA enough to eliminate aspect ratio-dependent divergence as reported by Hu et al. (2011). This does support our conclusion ignoring long cell lengths however, in order to keep the aspect ratio within a reasonable limit and ensure a linear fit is extrapolated. (EVEN THOUGH 48x8x8 HAS A SMALLER RATIO than 8x2x2?)

(WAFFLE ALERT) Ignoring the specifics of this study, we stress the importance of performing finite-size analysis when performing direct method calculations. Direct method cells spanning a range of lengths must be considered to find the linear regime for extrapolation. Cross-sectional area must be increased until the conductivity result converges. The same can be said about the Green–Kubo method, where the result converges with increasing volume. These effects vary with phonon mean-free path, sensitive to pressure, temperature, and compositional variations such as impurities. Completing finite-size effect analysis at conditions with the largest phonon mean-free path / thermal conductivity ensure all other conditions represent converged results. We believe classical molecular dynamics with interatomic potentials to be an excellent way of quantifying these effects quickly, performing ab initio methods (SHOULD I TAKE THIS SENTENCE OUT, NO PROOF OF THIS CLAIM).

Chapter 4

Modelling the thermal conductivity of $(Mg,Fe)SiO_3$ at the CMB

As stated earlier (REF), there are no are experiments that can reach the high pressures and temperatures necessary to represent the bottom of the lower mantle. The addition of impurities into minerals further complicates the matter, as pressure, temperature, and composition must be considered for proper evaluation.

DISCUSS/RE-ITERATE EARLIER-DISCUSSED SEMI-RELEVANT EXPERIMENTS HERE, MANTHILAKE

4.1 Simulating the effect of atomic impurities

The bulk of the lower mantle comprises bridgmanite (X%, and its post-perovskite high-pressure phase), periclase (Y%), along with others (Z%) such as calcium silicate perovskite $CaSiO_3$. The composition can vary within these mineral archetypes, significantly the concentration of iron impurities. Magnesium is replaced with iron in $MgSiO_3$ and MgO compositions, leading to $FeSiO_3$ and FeO endmembers. Aluminium can similarly be subsituted for Magnesium (((REF))) (Mg^{2+} + Si^{4+} = Al^{3+} + Al^{3+} or Al^{3+} + Fe^{3+}).

Impurities reduce thermal conductivity by providing more opportunities for phonon scattering events. An impurity is an irregularity to a propagating phonon, much like a speedbump to a car. They have different properties to the atoms the phonon expects to meet from crystal regularity, namely mass and their bonds with neighbouring atoms. For this reason that the thermal conductivity of a solid solution is lower at intermediate compositions than at the endmembers. Even if one endmember has lower conductivity than the other, an irregular mix of the two can produce even lower values.

4.1.1 How does iron behave?

I use two methods to introduce iron impurities to my bridgmanite models. The first approach is to simply create a magnesium atom with the mass of an iron atom, without changing any coefficients of the interatomic potentials from Oganov et al. (2000). Despite being an obviously "quick and dirty" method, (I will show) this is a reasonable first-order approximation(((PROVE IT!?))). As the variation in mass number from Mg to Fe is large (24 to 56, a 133% increase), it is likely to change the behaviour of the system more than a subtle change in the atomic interactions.

MENTION AMMANN IRON STUFF HERE

The second approach to add Fe into the $MgSiO_3$ system is to fit interatomic potentials, as well as using the aforementioned mass change for a more realistic model.

I adapted the Oganov et al. (2000) MgSiO$_3$ Buckingham interatomic potential (U) to include the Fe-O interation. I determined two short-range potential parameters, b and ρ, shown in Eq. 11 from Oganov et al. (2000),

$$U_{ij}\left(R_{ij}\right) = \frac{z_i z_j}{R_{ij}} + b_{ij}\exp\left(-\frac{R_{ij}}{\rho_{ij}}\right) - \frac{c_{ij}}{{R_{ij}}^6}, \tag{4.1}$$

where ij refers to an atom pair, R is interatomic distance, z is atomic charge, and c relates to the Van der Waals force (zero for non O-O interactions). We determine ρ in the same fashion as Oganov et al. (2000), calculated from the atomic first ionisation potentials,

$$\rho_{ij} = \frac{1.85}{\sqrt{I_i} + \sqrt{I_j}}. \tag{4.2}$$

b is constrained using the GULP code (Gale, 1997), using the calculated ρ value for Fe-O. We fit to the elasticity results of Parise and Wang (1990), an experimental study of (Mg$_{0.9}$,Fe$_{0.1}$)SiO$_3$ bridgmanite up to 433 K. Despite potential fitting being an improvement on solely changing mass (((PROVE IT!?))), it is still not perfect as the charge of our fitted Fe is not varied from the original Mg.

!!! Validate potentials

4.1.2 Where do the impurities go?

Iron is substituted with magnesium into the bridgmanite atomic structure. The unit cell contains 4 Mg atoms, and the smallest direct method cell I employ is a 6x2x2 supercell. Therefore the smallest amount of iron that can be added is 1/96 atoms, a concentration just over 1%. A simple script (((INCLUDE IN APPENDIX, MENTION MATLAB?))) is used to modify LAMMPS input files, randomly selecting a specified proportion of Mg atoms to be replaced with Fe. When a Mg atom changes to Fe, its mass and interatomic potential properties change.

Due to the microscopic nature of the system, we do not want all of the added iron to be concentrated together in the simulation cell, especially in a heat source/sink region (((ELABORATE WITH FIGURE?))). To avoid this we order Mg atoms by length along supercell, and change a single atom every so many. For example, changing 1/4 atoms is different to changing 24/96. The latter has a higher variance in Fe per unit length, and the former chooses one atom to swap for every four along the system. After iron is added, the standard direct method or Green-Kubo workflow is followed.

4.2 Making the mantle model

Due to uncertainty in the lower mantle's compositional distrubution, properties like thermal conductivity are averaged considering the relative abundance of each mineral component. There are also endmember relations to consider for each mineral, the concentration of impurities, and mineral phase transitions.

A simple weighted average (VRH?) can be used to combine the contributions of individual minerals, whereas mixing between endmembers is non-linear. Ohta et al. (2017) derive an equation for interpolating conductivity between mineral endmembers, specifically (Mg,Fe)O (ferro)periclase. I apply it to (Mg,Fe)SiO$_3$ perovskite [[[PRESUMABLY ALSO WORKS FOR bdg<->p-Pv?]]].

Okuda et al. (2017) present a temperature scaling relation for bridgmanite, which I apply to both Mg and Fe-endmembers. By having temperature-dependent values I am able to obtain an equation that gives thermal conductivity as a function of both temperature and composition, for a given (studied/fit?) endmember pair.

The aforementioned equation from Okuda et al. (2017) considers density, allowing conductivity to be determined as a function of temperature and pressure. In the examples I will present, I am only concerned with systems at 136 GPa. All density changes will result from thermal expansion SCIENCE HERE

4.2.1 Fitting the data

[Equations from Ohta et al., 2017 (eq. 7,8,9), and Okuda et al., 2017 (eq. 5)]

I want to determine lattice thermal conductivity as a function of temperature and composition, using calculated and fit constants. For the method I will use I need to know how the conductivity of endmember minerals changes with physical conditions. In order to keep temperature the only dependent variable, I will scale volume linerarly with temperature [FIGURE]. At this point I can scale the conductivity of an endmember with temperature within the fitted range (Okuda et al., 2017).

Considering Ohta et al. (2017), the linear interpolation between the conductivities of two endmembers can be perturbed, forming the trough characteristic of varying composition. While $FeSiO_3$ generally has a lower thermal conductivity than $MgSiO_3$, the minimum is located at an intermediate composition. The effect of impurity scattering is larger than inherent changes due to chemistry.

Compositional dependence

Ohta et al., 2017
* = already cited somewhere above

SEE STACKHOUSE 2015 EPSL SUPP. INFO. FOR MORE ON THIS EQUATION
Ohta eq. 7

$$\kappa_{latt} = \kappa_i \left(\frac{\omega_0}{\omega_M}\right) arctan \left(\frac{\omega_M}{\omega_0}\right) \tag{4.3}$$

κ_{latt} - output conductivity as function of t & x ($Wm^{-1}K^{-1}$), considering mineral specific parameters
κ_i - the composition-dependent conducitivity, if it were linearly interpolated between endmembers ($Wm^{-1}K^{-1}$)
ω_0/ω_M - temperature-dependent parameter to perturb κ_i, to create the "trough" trend in composition-dependent conductivity
ω_0 - *"the phonon frequency where the intrinsic mean free path is equal to that due to solute atoms"*
ω_M - *"the phonon frequency corresponding to the maximum of the acoustic branch of the phonon spectrum"*

The two components κ_i and ω_0/ω_M, are both temperature and composition-dependent. κ_i gives the compositionally-weighted average conductivity, a linear interpolation between endmembers at a certain temperature. ω_0/ω_M controls the conductivity decrease due to the impurity effect, the magnitude of which depends on the temperature and composition of interest.

By combining models for the temperate-dependence of MgSiO$_3$ and FeSiO$_3$-endmember conductivities, and the fit χ^T parameter, I obtain a function for conductivity of the lower mantle (136 GPa) as a function of just temperature and composition (as illustrated in Figure. 4.1).

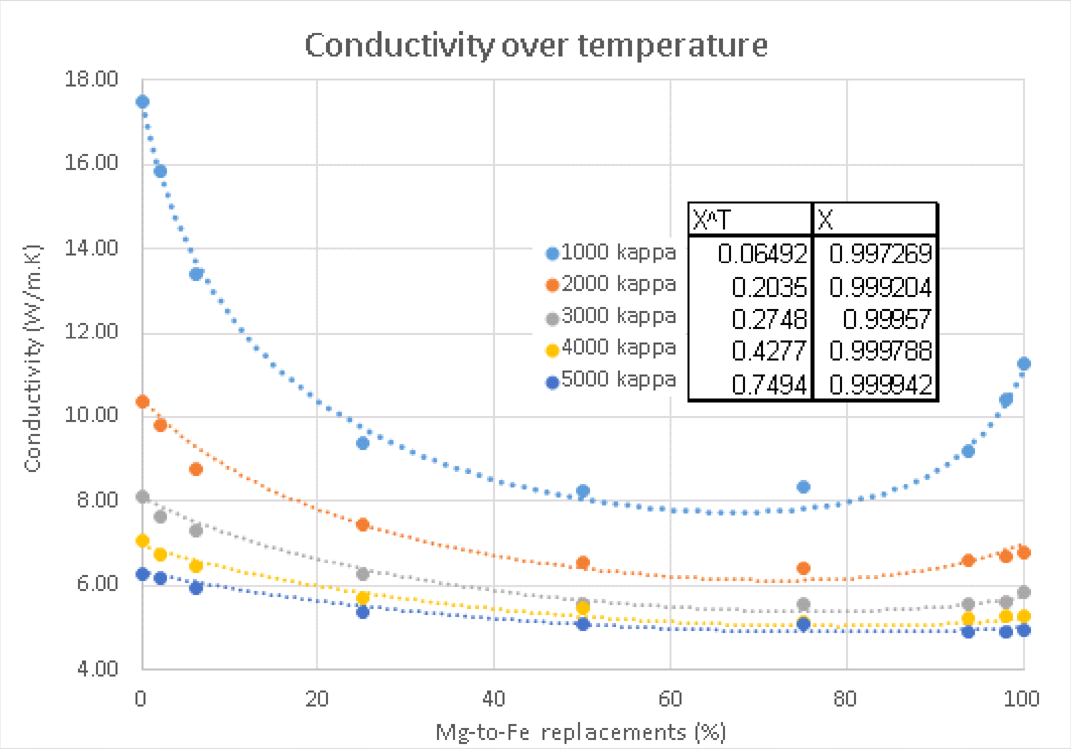

X^T	X
0.06492	0.997269
0.2035	0.999204
0.2748	0.99957
0.4277	0.999788
0.7494	0.999942

FIGURE 4.1: Each coloured dot series relates to a given temperature, the dotted fit lines are the model output.

Ohta eq. 8

$$\left(\frac{\omega_0}{\omega_M}\right)^2 = \frac{\chi^T}{C\,(1-C)} \tag{4.4}$$

*ω_0/ω_M - temperature-dependent parameter to perturb κ_i, to create the "trough" trend in composition-dependent conductivity
*ω_0 - *"the phonon frequency where the intrinsic mean free path is equal to that due to solute atoms"*
*ω_M - *"the phonon frequency corresponding to the maximum of the acoustic branch of the phonon spectrum"*
χ^T -temperature-dependent parameter to ...???
χ - *"a constant"*...
T - temperature of interest (K, default data fit between 1000 - 5000 K, but extrapolation should be reasonable)
C - composition mix of interest (dimensionless, values between 0 and 1)

The equation splits ω_0/ω_M into its temperature and composition-dependent components, where χ is a temperature-dependent variable. A value for χ is fit for all compositions at each temperature. $C\,(1-C)$ is largest when $C = 0.5$ *or* 50%, relating to the shape of the trough formed by this fit.

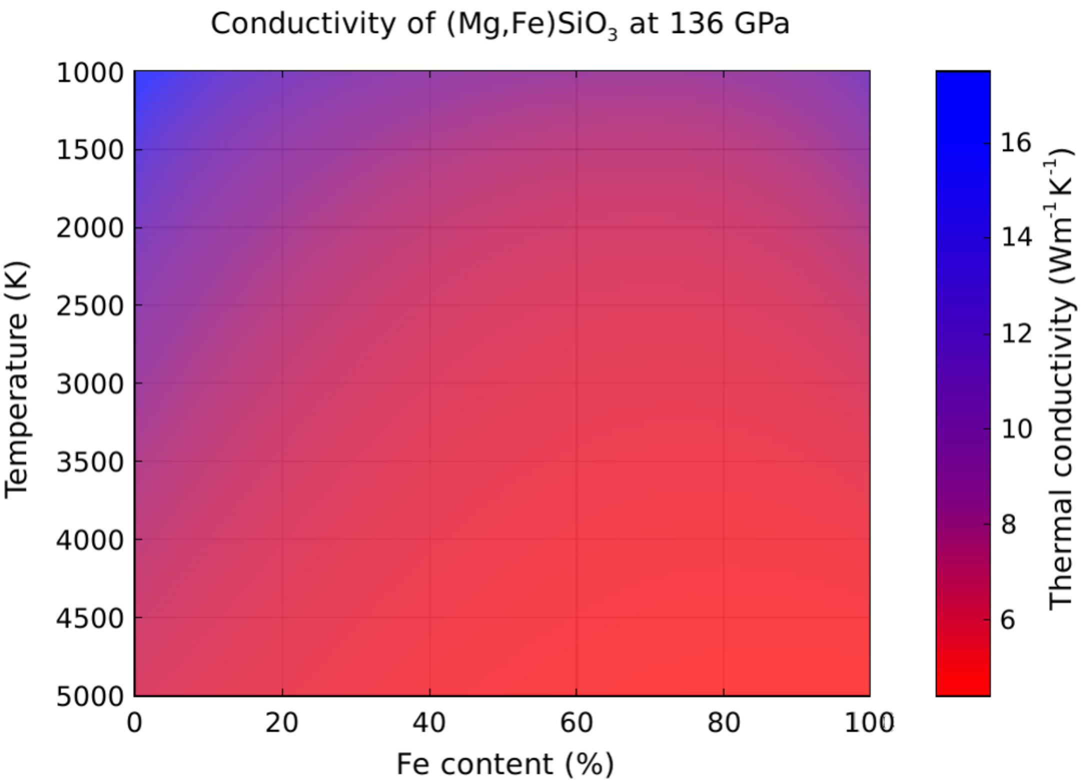

FIGURE 4.2: Modelled conductivity, shown plotted against temperature and composition. Note the sensitivity of the colour scale, showing low conductivities as dominant at high temperatures and intermediate compositions. High values are found only at low temperatures, and even then they rapidly decay and saturate to <8Wm^{-1}K^{-1}. Such conditions are unphysical at 136 GPa within the lower mantle.

χ^T scaling

$$\chi^T = AT^B \tag{4.5}$$

*χ^T -temperature-dependent parameter to . . . ???
*χ - *"a constant"*. . .
*T - temperature of interest (K, default data fit between 1000 - 5000 K, but extrapolation should be reasonable)
A - coefficient in χ^T variation with temperature
B - exponent in χ^T variation with temperature

In order to obtain an equation for conductivity at any mantle temperature, it is required that χ can be expressed as function of temperature. Figure 4.3 shows χ over T fit with a power law and 4th order polynomial, the former of which is a poor fit and the latter an egregious overfitting.

The lack of an obvious trend in χ against T can be countered by plotting χ^T over T, and fitting either a expontial or power law relationship (Figure 4.4). I use the power law-relationship as it represents the temperature-dependence better, both statistically and sensitivity-wise. The value of χ^T at high T has a lesser effect on the conductivity-composition relationship than at low T, where the power law fit matches the data closer. In Figure 4.3, we can see that either of the power law or exponential χ^T/T fits represent the data better than the χ/T relations.

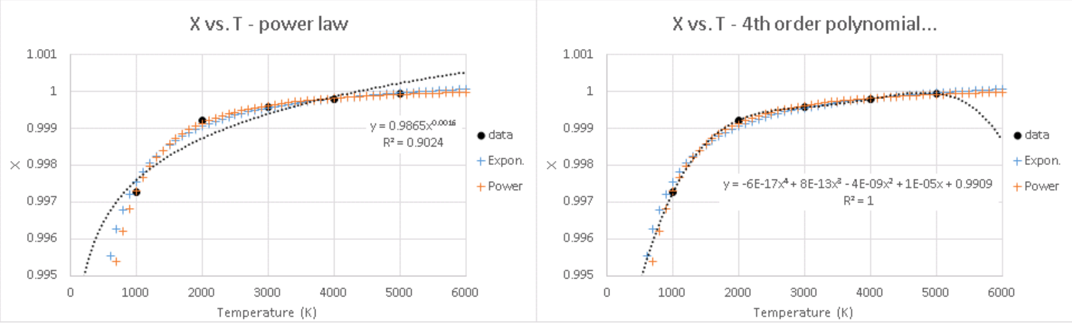

FIGURE 4.3: The fit χ values plotted against T, with power law (left) and 4th order polynomial (right) trendlines. Blue and orange series are the exponential and power law fits obtained from plotting χ^T/T (see Figure 4.4).

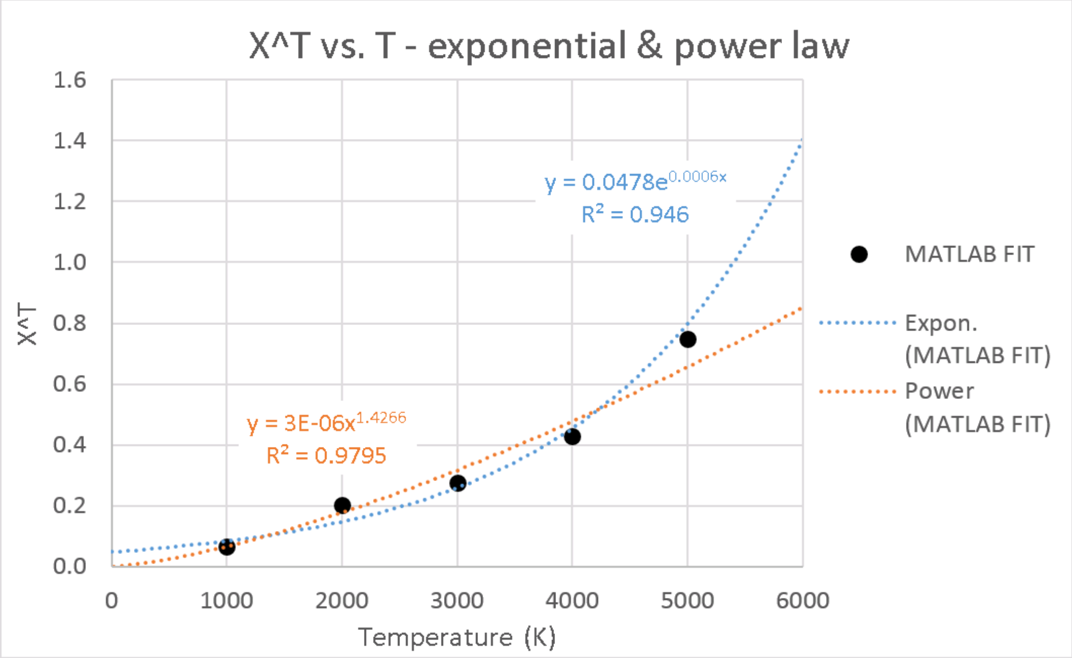

FIGURE 4.4: Exponential fit in blue (more curved), power law in orange (flatter)

Ohta eq. 9

$$\kappa_i = (1 - C)\,\kappa_{MgSiO_3} + C\,\kappa_{FeSiO_3} \tag{4.6}$$

*κ_i - the composition-dependent conducitivity, if it were linearly interpolated between endmembers (Wm^{-1}K^{-1})
*C - composition mix of interest (dimensionless, values between 0 and 1)
κ_{MgSiO_3} - temperature and volume-dependent conductivity for Mg endmember (Wm^{-1}K^{-1})
κ_{FeSiO_3} - temperature and volume-dependent conductivity for Fe endmember (Wm^{-1}K^{-1})

This equation describes the conductivity of an intermediate composition, assuming the relation is a simple weighted mean. C, in this case specifically, is the proportion of Fe atoms swapped into the system for Mg. The actual dependence of conductivity with composition is more complicated, this intermediate average value is adjusted for atomic-scale effects in Equation. 4.3 (Ohta et al., 2017, Eq. 7).

Temperature dependence

Okuda et al., 2017

Okuda eq. 5

$$\kappa_{adj} = \kappa_{ref} \left(\frac{\rho}{\rho_{ref}} \right)^{g} \left(\frac{T_{ref}}{T} \right)^{a} \tag{4.7}$$

κ_{adj} - temperature and density-dependent conductivity of an endmember ($\mathrm{Wm^{-1}K^{-1}}$)
κ_{ref} - reference conducitivty
T_{ref} - reference temperature
a - exponent controlling temperature-dependent conducitvity of an endmember
ρ_{ref} - reference density
g - exponent controlling density-dependent conducitvity of an endmember

Okuda et al. (2017) use a model for density and temperature-dependent conductivity (((from Manthilake 2011, REF???))), which utilises exponents obtained from REAL data / is calculated? (actually real numbers, only mine are fitted?). A reference value is scaled to infer conductivity at the conditions of interest, which in this case is temperature and pressure (via proxy using simulation cell volume/density).

Okuda eq. 5 modified

$$\kappa_{adj} = \kappa_{ref} \left(\frac{T_{ref}}{T} \right)^{a} \left(\frac{V_{ref}}{V} \right)^{h} \tag{4.8}$$

T_{ref} - temperature at which reference conductivity is calculated (K)
T - temperature of interest to interpolate (K, default data fit between 1000 - 5000 K, but extrapolation should be reasonable)
V_{ref} - reference volume of an endmember (E-30 $\mathrm{m^3}$)
V - temperature-dependent volume of an endmember (E-30 $\mathrm{m^3}$)
h - exponent controlling volume-dependent conducitvity of an endmember

I adapt Eq. 4.7 to consider volume instead of density (Eq. 4.8), where density and volume are inversely proportional. Varying a and h I fit this equation for both Mg and Fe endmembers, using reference values from 1000 K (see Figure 4.5). The purpose of this is to scale the conductivities needed for Eq. 4.6 to any temperature of interest.

Volume scaling ($y = mx + c$)

$$V = \frac{\partial V}{\partial T} T + V_{T_0} \tag{4.9}$$

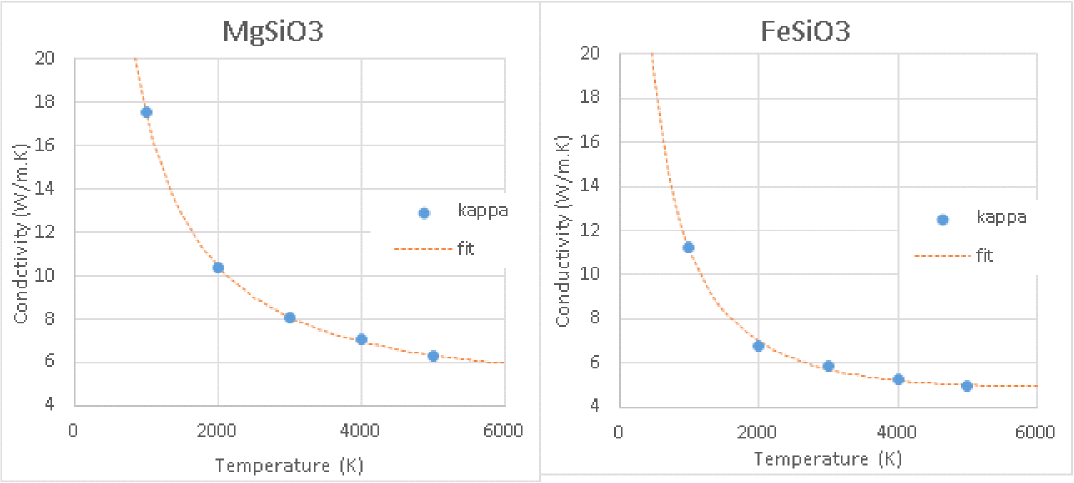

FIGURE 4.5

*V - temperature-dependent volume of an endmember (E-30 m^3)
$\partial V/\partial T$ - fit gradient, change of volume with temperature (E-30 m^3/K)
*T - temperature of interest (K, default data fit between 1000 - 5000 K, but extrapolation should be reasonable)
V_{T_0} - intercept volume for T=0 K (E-30 m^3)

I take Eq. 4.7 (Okuda et al., 2017, Eq. 5) a step further, by obtaining V in terms of T. This dependence is effectively linear over the temperatures considered (see Figure 4.6). With this, Eq. **??** can be made into a function of just temperature, meaning Eq. 4.3 (Ohta et al., 2017, Eq. 7) is dependent solely on temperature, composition, and fit or calculated constants.

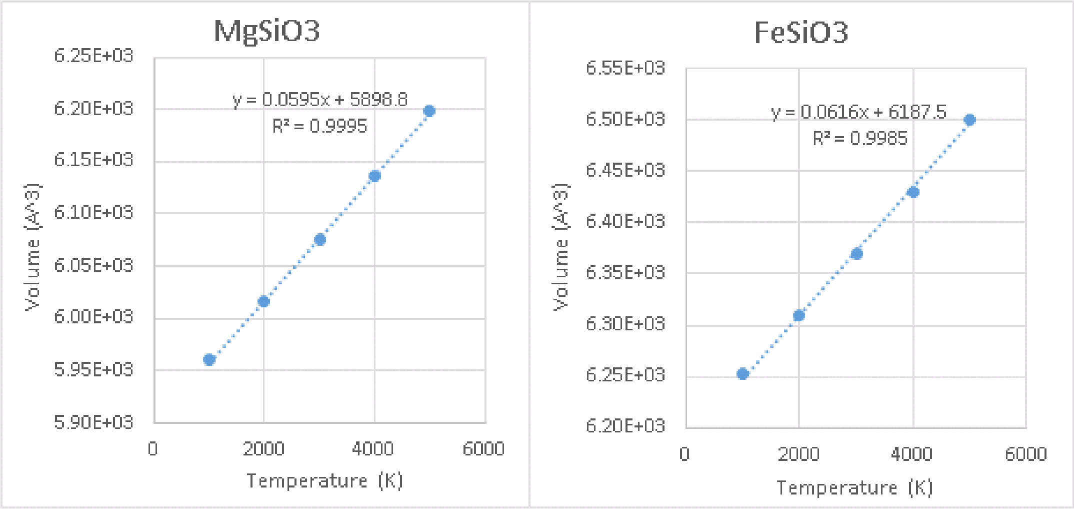

FIGURE 4.6: Number of atoms is kept constant for all volumes, data is obtained from GK calculations of a 4x4x3 simulation cell. Magnitude of volume isn't of interest, just the relative difference to the reference volume.

4.3 Results

Taking Green-Kubo results at the full range of lower mantle temperatures (1000-5000 K) and CMB pressure (136 GPa), I fit Equation 4.7 to obtain conductivity as a function of temperature for Mg and Fe silicate perovskite endmembers (Figure 4.7).

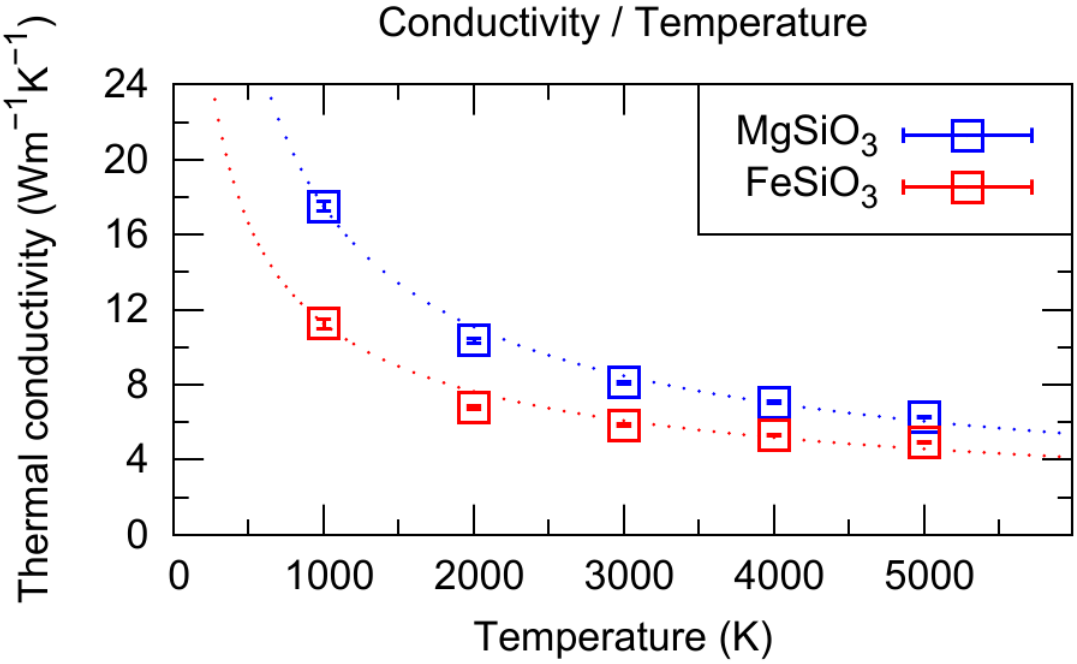

FIGURE 4.7: Data points are GK conductivity results, dotted line is the fit from Equation 4.8.

We also consider the effects of variable Mg:Fe across the same temperatures and pressures (Figure 4.8). Conductivity decreases sharply as Fe is introduced and reaches a plateau around intermediate compositions, then increases towards 100% Fe.

A simple interpolation between endmember conductivities is insufficient, the presence of a compositional mix has an effect. This effect is itself temperature-dependent, the trough-like trend flattens with increasing temperature. These temperature and compositional dependences can be combined, allowing conductivity to be determined for a range of possible CMB conditions (Figure 4.9).

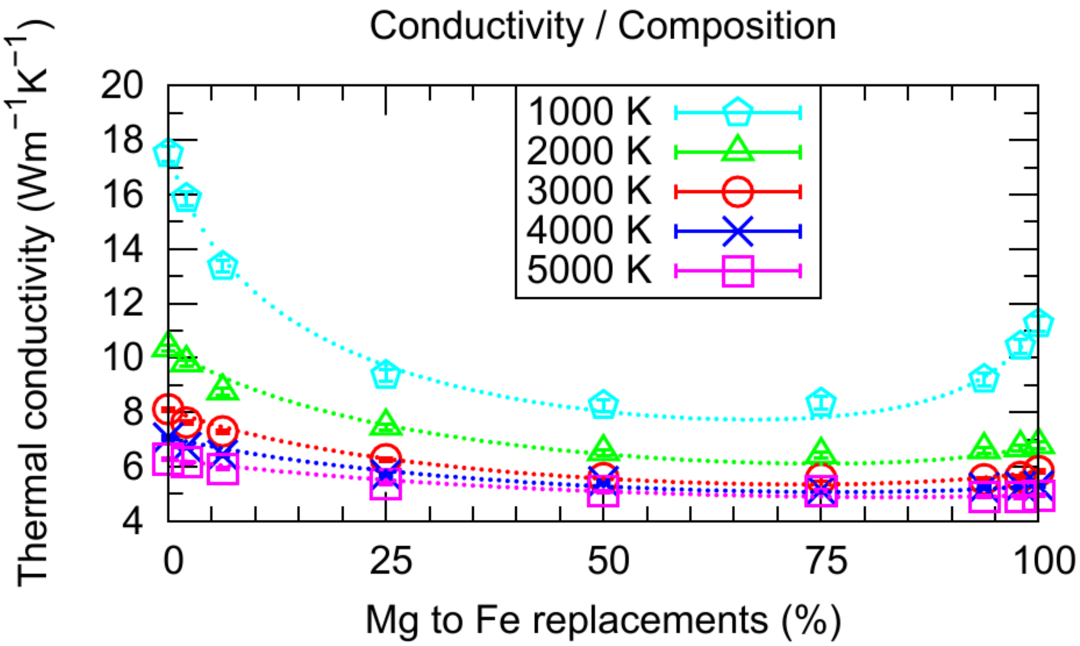

FIGURE 4.8: CAPTION

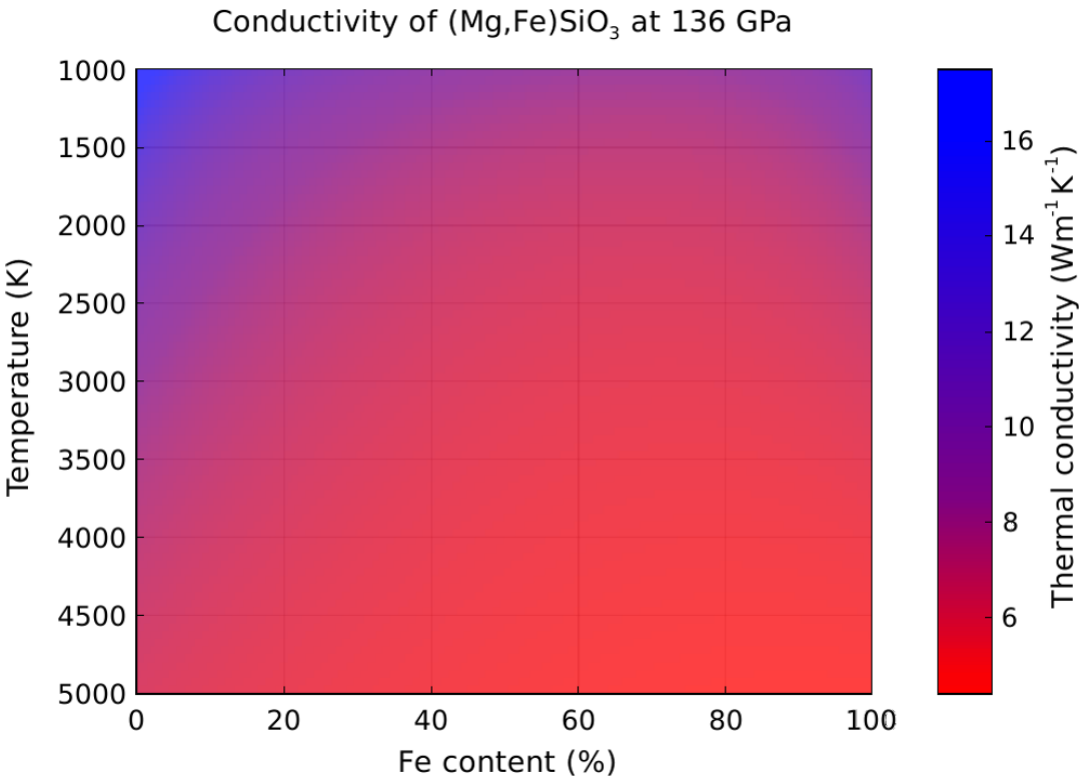

FIGURE 4.9: CAPTION

Chapter 5

Modelling the lower mantle with variable thermal conductivity

5.1 Main Section 1

Lorem ipsum dolor sit amet, consectetur adipiscing elit. Aliquam ultricies lacinia euismod. Nam tempus risus in dolor rhoncus in interdum enim tincidunt. Donec vel nunc neque. In condimentum ullamcorper quam non consequat. Fusce sagittis tempor feugiat. Fusce magna erat, molestie eu convallis ut, tempus sed arcu. Quisque molestie, ante a tincidunt ullamcorper, sapien enim dignissim lacus, in semper nibh erat lobortis purus. Integer dapibus ligula ac risus convallis pellentesque.

5.1.1 Subsection 1

Nunc posuere quam at lectus tristique eu ultrices augue venenatis. Vestibulum ante ipsum primis in faucibus orci luctus et ultrices posuere cubilia Curae; Aliquam erat volutpat. Vivamus sodales tortor eget quam adipiscing in vulputate ante ullamcorper. Sed eros ante, lacinia et sollicitudin et, aliquam sit amet augue. In hac habitasse platea dictumst.

Chapter 6

Summary/Discussion/Conclusion

6.1 Main Section 1

Lorem ipsum dolor sit amet, consectetur adipiscing elit. Aliquam ultricies lacinia euismod. Nam tempus risus in dolor rhoncus in interdum enim tincidunt. Donec vel nunc neque. In condimentum ullamcorper quam non consequat. Fusce sagittis tempor feugiat. Fusce magna erat, molestie eu convallis ut, tempus sed arcu. Quisque molestie, ante a tincidunt ullamcorper, sapien enim dignissim lacus, in semper nibh erat lobortis purus. Integer dapibus ligula ac risus convallis pellentesque.

6.1.1 Subsection 1

Nunc posuere quam at lectus tristique eu ultrices augue venenatis. Vestibulum ante ipsum primis in faucibus orci luctus et ultrices posuere cubilia Curae; Aliquam erat volutpat. Vivamus sodales tortor eget quam adipiscing in vulputate ante ullamcorper. Sed eros ante, lacinia et sollicitudin et, aliquam sit amet augue. In hac habitasse platea dictumst.

Appendix A

Frequently Asked Questions

A.1 How do I change the colors of links?

The color of links can be changed to your liking using:
`\hypersetup{urlcolor=red}`, or
`\hypersetup{citecolor=green}`, or
`\hypersetup{allcolor=blue}`.
If you want to completely hide the links, you can use:
`\hypersetup{allcolors=.}`, or even better:
`\hypersetup{hidelinks}`.
If you want to have obvious links in the PDF but not the printed text, use:
`\hypersetup{colorlinks=false}`.

Bibliography

Ammann, M. W. et al. (2014). “Variation of thermal conductivity and heat flux at the Earth’s core mantle boundary”. In: *Earth and Planetary Science Letters* 390, pp. 175–185. ISSN: 0012821X. DOI: 10.1016/j.epsl.2014.01.009. URL: http://linkinghub.elsevier.com/retrieve/pii/S0012821X14000120.

Brown, J. M. and R. G. McQueen (1986). “Phase Transitions, Grüneisen Parameter, and Elasticity for Shocked Iron Between 77 GPa and 400 GPa”. In: *Journal of Geophysical Research* 91.B7, pp. 7485–7494.

Dekura, H., T. Tsuchiya, and J. Tsuchiya (2013). “Ab initio Lattice Thermal Conductivity of MgSiO3 Perovskite as Found in Earth’s Lower Mantle”. In: *Physical Review Letters* 110, pp. 1–5. ISSN: 0031-9007. DOI: 10.1103/PhysRevLett.110.025904. URL: http://link.aps.org/doi/10.1103/PhysRevLett.110.025904.

Gale, J. D. (1997). “GULP: A computer program for the symmetry-adapted simulation of solids”. In: *J. Chem. Soc.* 93, pp. 629–637.

Goncharov, Alexander F. et al. (2009). “Thermal conductivity of lower-mantle minerals”. In: *Physics of the Earth and Planetary Interiors* 174.1-4, pp. 24–32. ISSN: 00319201. DOI: 10.1016/j.pepi.2008.07.033. URL: http://linkinghub.elsevier.com/retrieve/pii/S0031920108001945.

Green, M. S. (1954). “Markoff Random Processes and the Statistical Mechanics of Time-Dependent Phenomena. II. Irreversible Processes in Fluids”. In: *The Journal of Chemical Physics* 22.3, pp. 398–413. DOI: 10.1063/1.1740082.

Haigis, Volker (2013). “Trace elements in silicate melts and the thermal conductivity of the earth’s deep mantle: insights from atomistic modeling of geomaterials”. PhD thesis. Freien Universität Berlin. URL: http://d-nb.info/1031915087/.

Hofmeister, A. M. (1999). “Mantle Values of Thermal Conductivity and the Geotherm from Phonon Lifetimes”. In: *Science* 283, pp. 1699–1706. ISSN: 00368075. DOI: 10.1126/science.283.5408.1699. URL: http://www.sciencemag.org/cgi/doi/10.1126/science.283.5408.1699.

Howell, P. C. (2012). “Comparison of molecular dynamics methods and interatomic potentials for calculating the thermal conductivity of silicon.” In: *The Journal of chemical physics* 137.22, p. 224111. ISSN: 1089-7690. DOI: 10.1063/1.4767516. URL: http://www.ncbi.nlm.nih.gov/pubmed/23248991.

Hu, L., W. J. Evans, and P. Keblinski (2011). “One-dimensional phonon effects in direct molecular dynamics method for thermal conductivity determination”. In: *Journal of Applied Physics* 110.11, p. 113511. ISSN: 00218979. DOI: 10.1063/1.3660234. URL: http://scitation.aip.org/content/aip/journal/jap/110/11/10.1063/1.3660234.

Koker, N. de (2009). “Thermal Conductivity of MgO Periclase from Equilibrium First Principles Molecular Dynamics”. In: *Physical Review Letters* 103.12, pp. 1–4. DOI: 10.1103/PhysRevLett.103.125902.

Kubo, R. (1957). “Statistical-Mechanical Theory of Irreversible Processes. I.” In: *Journa; of the Physical Society of Japan* 12.6. DOI: 10.1143/JPSJ.12.570.

— (1966). “The fluctuation-dissipation theorem”. In: *Reports on Progress in Physics* 29.1, pp. 255–283.

Lay, T., J. Hernlund, and B. A. Buffett (2008). “Core–mantle boundary heat flow”. In: *Nature Geoscience* 1, pp. 25–32. ISSN: 1752-0894. DOI: `10.1038/ngeo.2007.44`. URL: `http://www.nature.com/doifinder/10.1038/ngeo.2007.44`.

Manthilake, G. M. et al. (2011). “Lattice thermal conductivity of lower mantle minerals and heat flux from Earth’s core.” In: *Proceedings of the National Academy of Sciences of the United States of America* 108, pp. 1–4. ISSN: 1091-6490. DOI: `10.1073/pnas.1110594108`. URL: `http://www.pubmedcentral.nih.gov/articlerender.fcgi?artid=3207700{\&}tool=pmcentrez{\&}rendertype=abstract`.

Müller-Plathe, F. (1997). “A simple nonequilibrium molecular dynamics method for calculating the thermal conductivity”. In: *The Journal of Chemical Physics* 106.14, p. 6082. ISSN: 00219606. DOI: `10.1063/1.473271`. URL: `http://scitation.aip.org/content/aip/journal/jcp/106/14/10.1063/1.473271`.

Nieto-Draghi, C. and J. B. Avalos (2013). “Non-equilibrium momentum exchange algorithm for molecular dynamics simulation of heat flow in multicomponent systems”. In: *Molecular Physics* 101.14, pp. 2303–2307. DOI: `10.1080/0026897031000154338`.

Oganov, A. R., J. P. Brodholt, and D. G. Price (2000). “Comparative study of quasiharmonic lattice dynamics, molecular dynamics and Debye model applied to MgSiO3 perovskite”. In: *Physics of the Earth and Planetary Interiors* 122, pp. 277–288. URL: `http://www.sciencedirect.com/science/article/pii/S0031920100001977`.

Ohta, K. et al. (2012). “Lattice thermal conductivity of MgSiO3 perovskite and post-perovskite at the core–mantle boundary”. In: *Earth and Planetary Science Letters* 349-350, pp. 109–115. ISSN: 0012821X. DOI: `10.1016/j.epsl.2012.06.043`. URL: `http://linkinghub.elsevier.com/retrieve/pii/S0012821X12003354`.

Ohta, Kenji et al. (2017). “Thermal conductivity of ferropericlase in the Earth’s lower mantle”. In: *Earth and Planetary Science Letters* 465, pp. 29–37. ISSN: 0012821X. DOI: `10.1016/j.epsl.2017.02.030`. URL: `http://dx.doi.org/10.1016/j.epsl.2017.02.030`.

Okuda, Yoshiyuki et al. (2017). “The effect of iron and aluminum incorporation on lattice thermal conductivity of bridgmanite at the Earth’s lower mantle”. In: *Earth and Planetary Science Letters* 474.September, pp. 25–31. ISSN: 0012821X. DOI: `10.1016/j.epsl.2017.06.022`. URL: `http://dx.doi.org/10.1016/j.epsl.2017.06.022`.

Osako, M. and E. Ito (1991). “Thermal diffusivity of MgSiO3 perovskite”. In: *Geophysical Research Letters* 18, pp. 239–242. URL: `http://onlinelibrary.wiley.com/doi/10.1029/91GL00212/full`.

Parise, J B and Y Wang (1990). “of Mg substitutes for Si in the octahedral (Bhsite , with a x • Mg Fe + XB The use x • Fe x • Mg = This study ; The refined Mg / Fe , For data”. In: *October* 12, pp. 2089–2092.

Plimpton, S. (1995). “Fast Parallel Algorithms for Short – Range Molecular Dynamics”. In: *Journal of Computational Physics* 117, pp. 1–19. ISSN: 00219991. DOI: `10.1006/jcph.1995.1039`.

Schelling, Patrick K., Simon R. Phillpot, and Pawel Keblinski (2002). “Comparison of atomic-level simulation methods for computing thermal conductivity”. In: *Physical Review B* 65.14, p. 144306. ISSN: 1098-0121. DOI: `10.1103/PhysRevB.65.144306`. URL: `http://link.aps.org/doi/10.1103/PhysRevB.65.144306`.

Sellan, D. P. et al. (2010). “Size effects in molecular dynamics thermal conductivity predictions”. In: *Physical Review B* 81, pp. 1–10. ISSN: 1098-0121. DOI: `10.1103/PhysRevB.81.214305`. URL: `http://link.aps.org/doi/10.1103/PhysRevB.81.214305`.

Snyder, G Jeffrey and Eric S Toberer (2008). “Complex thermoelectric materials”. In: *Nature materials* 7.2, pp. 105–114. ISSN: 1476-1122. DOI: `10.1038/nmat2090`. arXiv: `1512.00567`.

Stackhouse, S. and L. Stixrude (2010). “Theoretical Methods for Calculating the Lattice Thermal Conductivity of Minerals”. In: *Reviews in Mineralogy and Geochemistry* 71, pp. 253–269. ISSN: 1529-6466. DOI: `10.2138/rmg.2010.71.12`. URL: `http://rimg.geoscienceworld.org/cgi/doi/10.2138/rmg.2010.71.12`.

Stackhouse, Stephen, Lars Stixrude, and Bijaya B Karki (2015). “First-principles calculations of the lattice thermal conductivity of the lower mantle”. In: *Earth And Planetary Science Letters* 427, pp. 11–17. ISSN: 0012821X. DOI: `10.1016/j.epsl.2015.06.050`. URL: `http://dx.doi.org/10.1016/j.epsl.2015.06.050`.

Tang, X. et al. (2014). “The thermal conductivity of the Earth’s lower mantle”. In: *Geophysical Research Letters* 41, pp. 2746–2752. DOI: `10.1002/2014GL059385.Received`. URL: `http://onlinelibrary.wiley.com/doi/10.1002/2014GL059385/pdf`.

Tang, Xiaoli and Jianjun Dong (2009). “Pressure dependence of harmonic and anharmonic lattice dynamics in MgO: A first-principles calculation and implications for lattice thermal conductivity”. In: *Physics of the Earth and Planetary Interiors* 174.1-4, pp. 33–38. ISSN: 00319201. DOI: `10.1016/j.pepi.2008.10.003`.

Thomas, J. A., R. M. Iutzi, and A. J. H. McGaughey (2010). “Thermal conductivity and phonon transport in empty and water-filled carbon nanotubes”. In: *Physical Review B - Condensed Matter and Materials Physics* 81.4, pp. 1–7. ISSN: 10980121. DOI: `10.1103/PhysRevB.81.045413`.

Tosi, Nicola et al. (2013). “Mantle dynamics with pressure- and temperature-dependent thermal expansivity and conductivity”. In: *Physics of the Earth and Planetary Interiors* 217, pp. 48–58. ISSN: 00319201. DOI: `10.1016/j.pepi.2013.02.004`. URL: `http://dx.doi.org/10.1016/j.pepi.2013.02.004`.